27 May 2010, 4:30 pm - 6:20 pm

Effect of a Slope on the Dynamic Properties of Diluvial Terrace

Shoichi Nakai
Chiba University, Japan

Yoko Nagata
Japan Conservation Engineers Co. Ltd., Japan

Toru Sekiguchi
Chiba University, Japan


Fifth International Conference on
Recent Advances in Geotechnical Earthquake Engineering and Soil Dynamics
and Symposium in Honor of Professor I.M. Idriss
May 24-29, 2010 • San Diego, California

EFFECT OF A SLOPE ON THE DYNAMIC PROPERTIES OF DILUVIAL TERRACE

Shoichi Nakai
Chiba University
Chiba-Japan 263-8522

Yoko Nagata
Japan Conservation Engineers Co. Ltd.
Tokyo-Japan 105-0001

Toru Sekiguchi
Chiba University
Chiba-Japan 263-8522

ABSTRACT

It is well known that landform influences the behavior of the ground during earthquakes. The objective of this study is to clarify the effect of a slope on the dynamic properties of diluvial terrace based on ground investigations, seismic motion observations and two-dimensional finite element analyses, by choosing a target area that has a landform typical to the southern Kanto plain in Japan. Through the study, the followings were found: (1) Due to a weak soil along the slope, amplification becomes very large, but the area of influence is relatively small. (2) Amplification due to ground irregularity itself is relatively small, but the area of influence is fairly large. (3) It should be noted that the possibility of slope failure during an earthquake becomes very large at the slope when a weak soil exists along the slope.

INTRODUCTION

It is essential to know the condition of the ground when considering earthquake disaster mitigation. It is well known that the surface soil condition and micro topography (landform) influence the seismic intensity of the ground and hence impact structural damage to the buildings and civil infrastructure during earthquakes. However, obtaining information on the ground condition, such as soil profiles, over a wide area is not an easy task. One of the effective approaches to estimate the ground condition is to consult topographic maps and examine the type of micro landform (Matsuoka and Midorikawa, 1994). An alternative is to look at land use and vegetation, especially in the old times, based on the fact that land use in the old times reflects the geological condition which has not been altered by human (e.g. Nakai, et al., 2002). These approaches work well when discussing an earthquake disaster as a whole, in that the dynamic properties are evaluated based on the one-dimensional analysis. However, when it comes to a detailed damage distribution in a smaller area, for example, landform itself plays an important role. It has been pointed out that two or three-dimensional analysis may be required at the boundary between the two landforms (e.g. Nakai et al., 2004).

A number of earthquake-induced failures have occurred at the top of slopes. In fact, during 1987 East Off Chiba Prefecture earthquake, it was reported that many slopes collapsed at the edge of a terrace, and during 1999 Chi-Chi earthquake in Taiwan, about 70% of earthquake-induced landslides originated at the upper part of slopes (Wang et al., 2004). In addition, shaking table tests with a large-scale slope model showed an increase in the response acceleration at the upper part of a slope (Asano et al., 2003).

Several studies have been made on the effect of slopes on the dynamic properties of the ground. For example, in the recent studies based on the three-dimensional finite element analyses, Kurita et al., 2005, and Asano et al., 2006, have pointed out that ground motions during an earthquake can be amplified at the ridge of mountains. According to Nagata et al., 2006 and 2008, however, the geometric configuration alone cannot explain the effect of landform on the dynamic characteristics of the ground. This implies that a further investigation on this effect is needed.

The objective of this study is to examine dynamic characteristics of the ground near a slope located at the edge of diluvial terrace, which is a common landform in and near the Tokyo metropolitan area, based on microtremor and seismic motion observations as well as two-dimensional finite element analyses.

OBSERVATIONS AND MEASUREMENTS

Target Area

Throughout this study, Chiba city is selected as a target area. Chiba is located at about 40 km east of Tokyo. Figure 1 shows landform classification in central Chiba (based on Chiba Pref. Gov. 1980) and also shows the locations of microtremor and seismic motion measurements. The landforms of his area consists of diluvial terrace, alluvial plain and reclaimed ground.

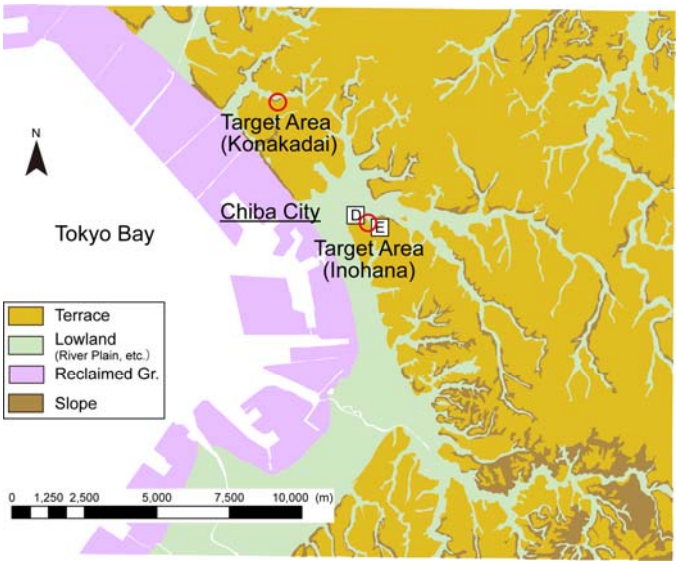

Fig. 1. Target area (Chiba city).

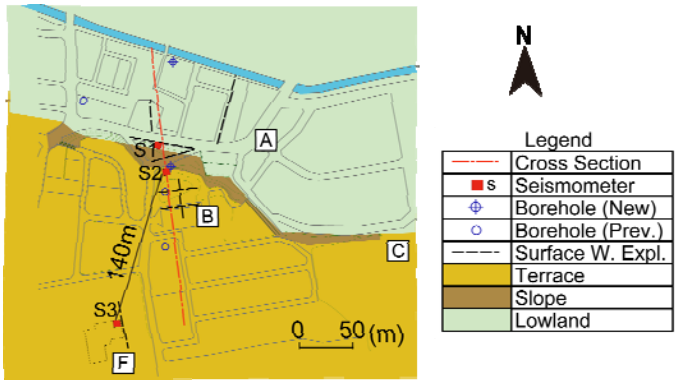

Fig. 2. Target area (Konakadai; see Fig. 1.).

Diluvial terrace is covered with a volcanic cohesive soil called Kanto loam with the thickness of about 5 m. Under the Kanto loam formation, there is a heap of diluvial sands, which are called Narita formation of Shimousa group. Alluvial plain is normally covered with soft alluvial soils.

Microtremor measurements were conducted at six sites as shown in Figs. 1 and 2 (sites A to F). Of these, four sites are located at the edge of a terrace; one is in a valley plain near a slope, and another one is in the middle of a terrace. Three seismometers are installed at S1, S2 and S3 locations. Table 1 summarizes the landform of each observation site.

Table 1. Observation sites.

Site	Observation	Landform
A	Microtremor	Valley plain
B	Microtremor	Terrace (edge)
C	Microtremor	Terrace (edge)
D	Microtremor	Terrace (edge)
E	Microtremor	Terrace (edge)
F	Microtremor	Terrace
S1	Seismic motion	Foot of slope
S2	Seismic motion	Terrace (edge)
S2	Seismic motion	Terrace

Sites A, B, C and seismometer observation locations (S1 and S2) are situated in the northern part of Chiba city. There is a small valley plain of about 200 m width. Site A and S1 point are located in the lowland (plain) and sites B, C and point S2 are located in the upland (terrace). The area between sites A and B is a slope that has about 10 m height and the inclination of about 25 degrees.

Sites D and E are located on a terrace in the southern part of Chiba city. There is a river plain of about 2 km width. Site D is located in a terrace that borders a river plain, while site E is in a terrace that borders a branch of a river. The slope between the lowland and site E (terrace) is an artificially cut slope of about 20 m height.

Results of Microtremor Measurements

Relationship between Distance from Slope and Predominant Frequency. Microtremor measurements were carried out at six sites shown in Figs. 1 and 2. The observation sites are located at four landforms; valley plain, terrace near a natural slope, terrace near a cut slope, and the middle of a terrace. Figure 3 shows horizontal to vertical Fourier spectral ratios, or *H/V* spectra, obtained from microtremor measurements at each landform.

At site A (located in the valley plain), it is observed that the predominant frequency of an *H/V* spectrum changes to lower values in accordance with the distance from the foot of a slope. This means that the depth of an alluvial deposit increases. At site B (located at the edge of a terrace), *H/V* spectra show a lot of variations making it difficult to choose predominant frequencies. On the other hand, *H/V* spectra observed at site E (located at the edge of a terrace) show a

small variation, where variations of predominant frequencies are small. At site F (located in a terrace), *H/V* spectra show almost no change.

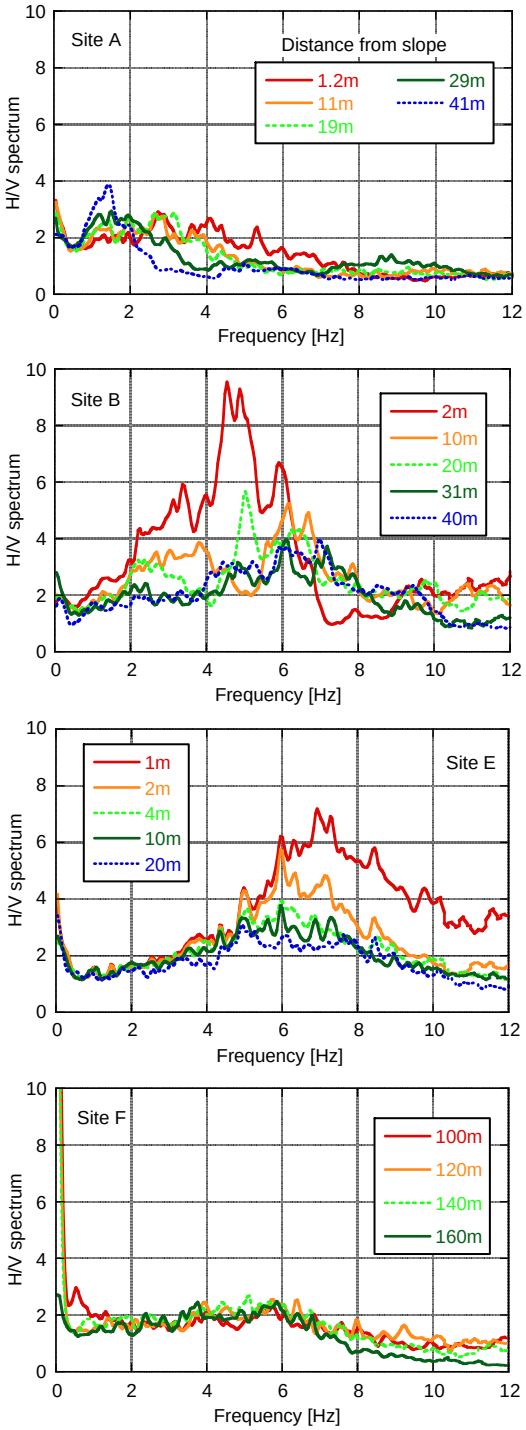

Fig. 3. H/V spectra of microtremor observations at different landforms (A:Valley plain, B:Terrace near a natural slope, E:Terrace near a cut slope and F:Terrace).

Figure 4 shows relations between the distance from a slope at the edge of a terrace and predominant frequencies of *H/V* spectra at B, C, and D. They show one peak at few meters from the slope, then two emerging peaks are found, and finally one peak remains at larger distances from the slope. It is found that the predominant frequencies of *H/V* spectra change to higher values in accordance with the distance from the shoulder of a slope in the case of a natural slope.

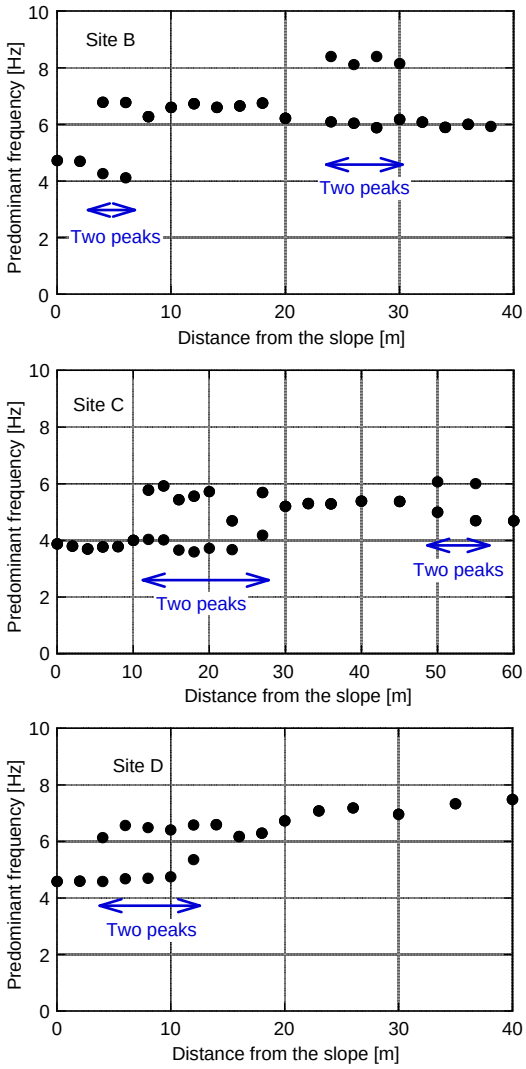

Fig. 4. Relationship between the distance from a slope and predominant frequencies of H/V spectra at the edge of a terrace.

Comparison with the Results of Ground Investigation. At site B (the edge of a terrace), a variety of soil investigations including surface wave explorations and PS loggings were performed to investigate detailed ground conditions. Figure 5 shows a cross sectional view of the ground of this site, constructed from these investigation results. According to Figs. 4 and 5, the distribution of shear wave velocity

(hereafter, *Vs*) and the predominant frequency have a sudden change at the distance of 20 m from the slope. *H/V* spectra also change due to the variation of the ground condition. Other sites near a slope, for example site C, although they do not have ground investigation data, *H/V* spectra show a similar tendency as the one at site B. Therefore, it can be concluded that the two areas have similar ground conditions. Non homogenous ground conditions were probably originated by the sedimentation and climate change in this area in the old times.

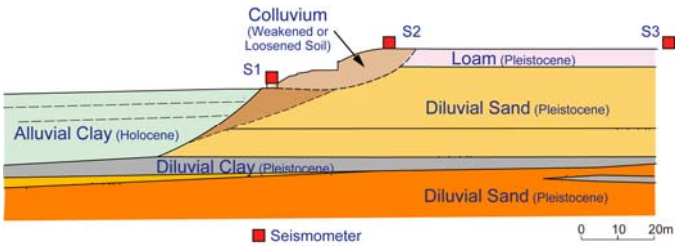

Fig. 5. Soil Profile of Site B.

Site E is located on a terrace near a slope as in the case of site B. However, at site E, the change of the predominant frequency is small. Only the peak of *H/V* spectra changes to lower values. The reason for this phenomenon could be that the sedimentation condition of the soil layers in this area was relatively uniform. Also, the high peaks of *H/V* spectra near the slope may be due to the existence of soft soil deposits.

Results of Seismic Motion Observations

Observed Earthquake Ground Motions. Seismic motions were observed at 3 locations as shown in Fig. 2. Table 2 shows the summary of the observed earthquakes. The seismic motions were observed for eight earthquakes at S1 and S2 locations, four earthquakes at S3. The slope between S1 and S2 locations has about 10 m height and the inclination of about 25 degrees. The S3 location is in the central part of the terrace. According to the observation, maximum accelerations recorded at S2 are twice as large compared with other locations.

Table 2. Summary of observed earthquakes.

No	Epicenter			Magnitude	DATE	Max Acceleration(ga		
	North latitude	East longitude	Depth (km)			S1	S2	S3
1	36° 2.3'	139° 53.3'	46	5.3	05/02/16	34	90	37
2	35° 43.6'	140° 37.2'	52	6.1	05/04/11	36	73	28
3	35° 37.8'	140° 4.8'	72	4.5	05/06/09	34	83	---
4	35° 44.0'	140° 41.6'	51	5.6	05/06/20	26	71	---
5	35° 34.9'	140° 8.3'	73	6	05/07/23	158	321	160
6	38° 8.9'	142° 16.6'	42	7.2	05/08/16	20	48	---
7	36° 2.3'	139° 56.2'	47	5.1	05/10/16	20	34	---
8	36° 22.9'	141° 2.5'	48	6.3	05/10/19	26	73	23
Seismometer	**North latitude**	**East longitude**	[Section]					
S1,S2	35°38.3'	140°6'						
S3	35°37.3'	140°6.4'						

Difference from the Viewpoint of Landform. The Fourier spectra of recorded ground motions are shown in Fig. 6. Fourier spectral ratios between the two sites are shown in Fig. 7. It can be pointed out from these figures that:

- Both *H/V* spectra of microtremors and seismic motions show similar tendencies, for example peak and dip frequencies. In addition, most of the Fourier spectra of the seismic motions have similar tendencies.

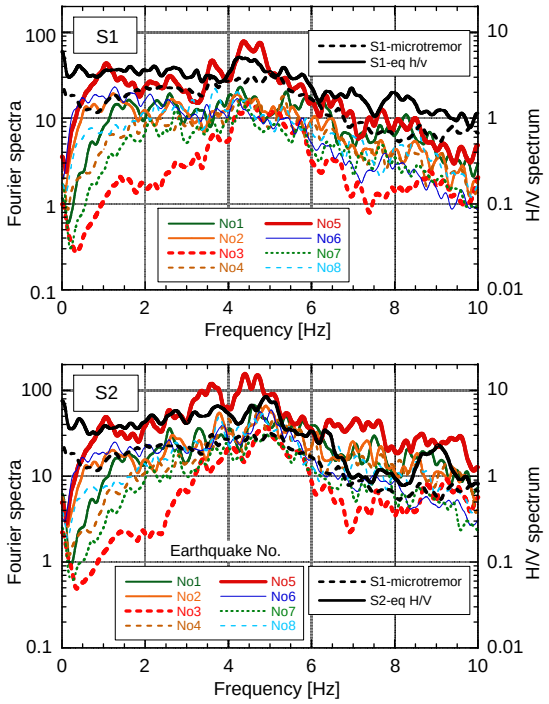

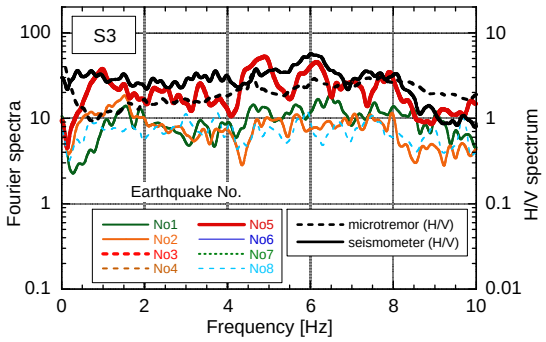

Fig. 6. Comparison among Fourier spectra (horizontal direction) of earthquake motions, microtremor H/V spectra and seismic motion H/V spectra (average of 4 to 8 records).

- Fourier spectra at S1 (the foot of a slope) tend to have a dip at about 3.5 Hz and a peak at about 4.2 Hz. Fourier spectra at S2 (the edge of a terrace) tend to have a dip between 4.0 and 4.2 Hz and have a peak between 4.5 and 5.0 Hz. It seems that Fourier spectral peaks and dips at S2 appear at frequencies 0.5 Hz higher than S1.
- Fourier and *H/V* spectra of earthquake No.5, during which the largest acceleration was recorded, have a peak between 4.5 to 5.0 Hz at all locations.

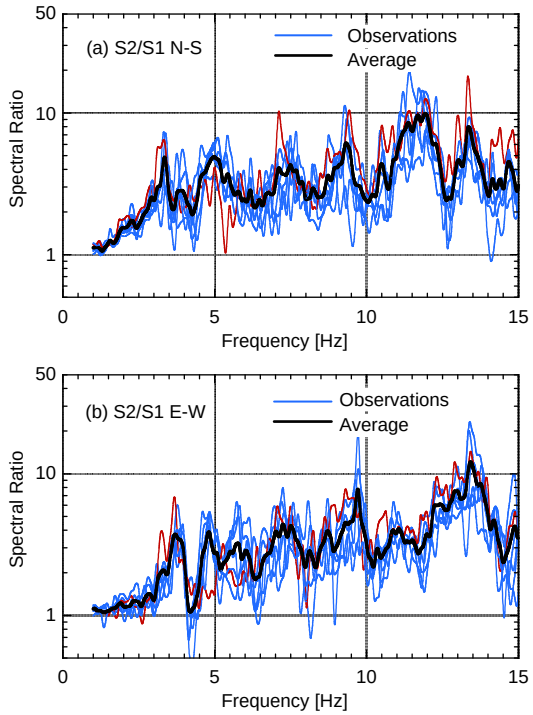

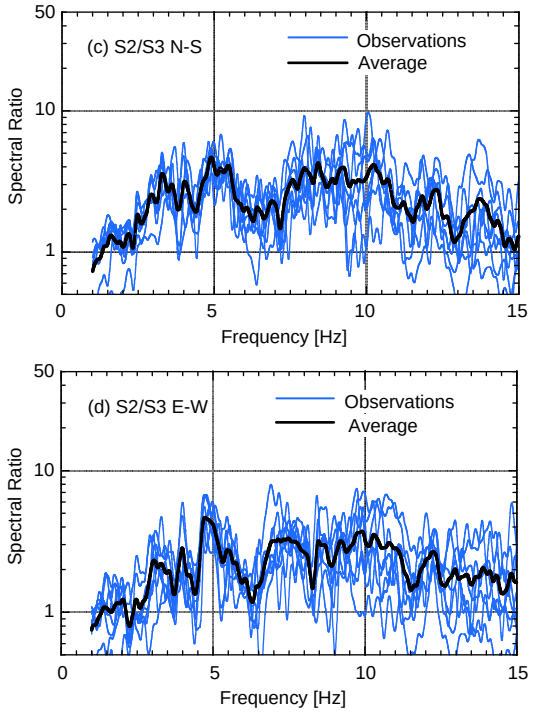

Fig. 7. Fourier spectral ratio between two sites.

- At S3 location (middle of a terrace), Fourier and *H/V* spectra show very little frequency dependency.
- In the low frequency range, Fourier spectra at S1, S2 and S3 show a similar behavior.
- S2 gives higher spectral intensities in the frequency range of 2 to 6 Hz, while S3 gives lower spectral intensities in the same frequency range, when compared to other locations. S1 is the lowest for higher frequencies above 6 Hz. S2 is the highest for all frequencies.

EFFECT OF A SLOPE ON THE DYNAMIC PROPERTIES OF THE GROUND

According to the discussion given in the previous chapter, it is suggested that a weakened soil along a slope in the natural condition influences the dynamic characteristics of the ground. In this chapter, this effect of a lope is examined in detail based on the two-dimensional finite element analysis of simplified soil models. So far, a few studies have been reported on this subject with a two-layered soil model (Kobayashi et al., 1993, and BRJ, 1995).

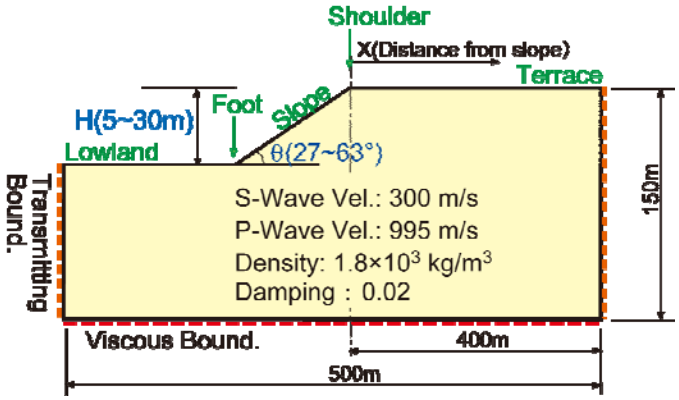

Fig. 8. Schematic illustration of a model used in finite element analyses.

Effect of a Slope: Uniform Soil

Analysis Model. In order to examine the effect of the existence of a slope, two-dimensional finite element analyses of a simple uniform soil model with a slope have been carried out, as shown in Fig. 8. Two parameters that describe the configuration of the slope were considered in the analysis: the inclination and height of the slope. As indicated in the figure, the upper part of the ground is called a terrace and the lower part of the ground is called a lowland in this study. Analyses have been conducted in the frequency domain with the use of so-called transmitting boundaries at both sides and dashpots at the bottom boundary.

Effect of the Height of a Slope. The height of 5, 10, 20 and 30 m was considered. Two different kinds of input wave were applied to the model at the bottom boundary as upward incident waves. The input wave 1 is an artificial ground motion and the input wave 2 is an actual record. The maximum acceleration was set to 1.0 m/s^2 for both waves.

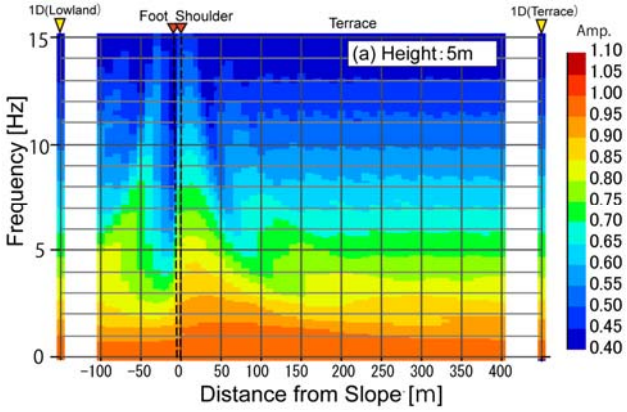

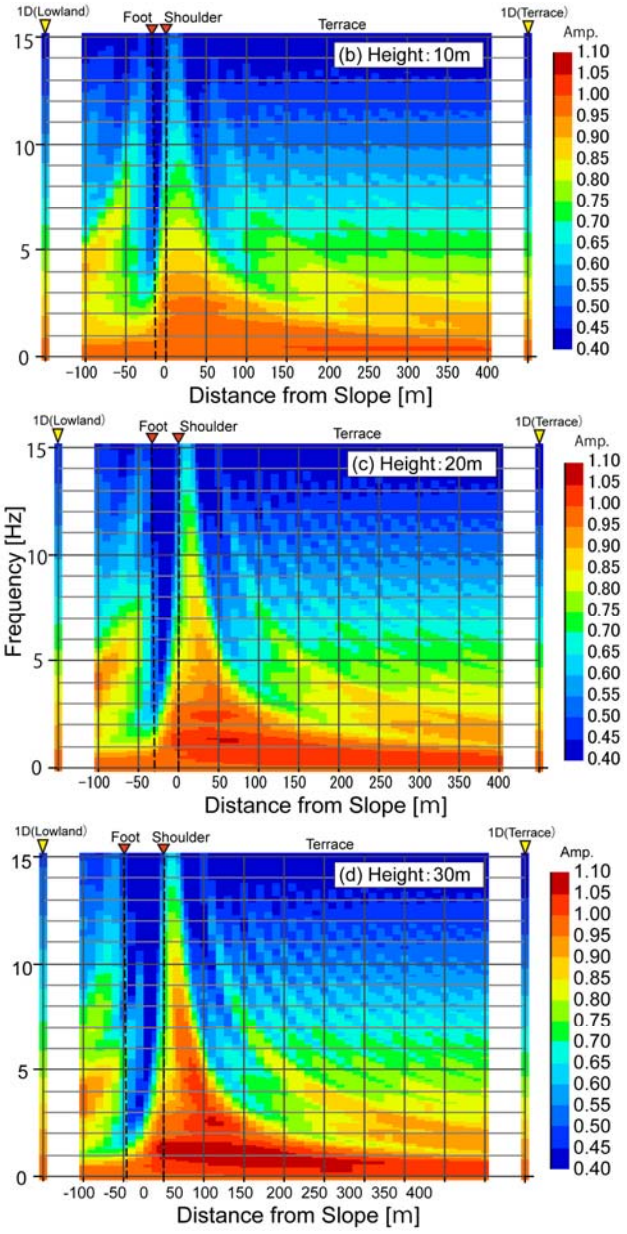

Fig. 9. Distribution of transfer functions on the ground surface (red color indicates larger amplification).

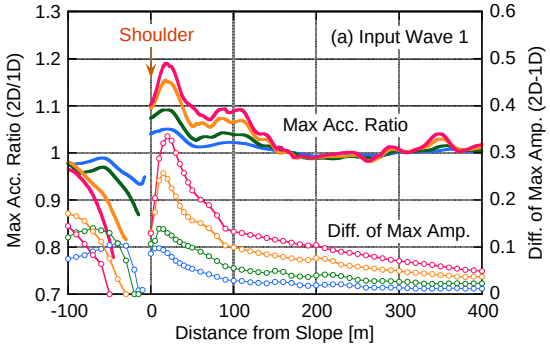

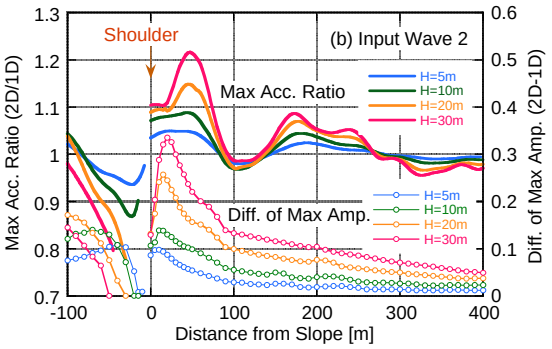

Fig. 10. Distribution of maximum response accelerations on the ground surface (also shown are the differences between 2-D and 1-D analyses).

Figure 9 shows the amplification function on the ground surface with respect to the input motion. From this figure, it can be seen that the frequency dependency of the amplification function changes according to the distance from the slope but the overall characteristics do not change that much regardless of the height of the slope. The peak value itself, however, increases as the height increases. The affected area due to the slope becomes large when the height is large. It is worthy of note that amplification is suppressed along the slope and at its foot.

Figure 10 shows the distribution of the ratio between the maximum acceleration along the ground surface and that of the input wave. According to this figure, it is seen that the ratio becomes large on the terrace and small at the foot of the slope when the height of the slope is large. It is noted that the maximum ratio appears at the terrace close to the shoulder but not at the shoulder itself. This phenomenon is harmonious with the previous study (Hayakawa, 1996) and may have some impact on the seismicity of the ground during earthquakes.

Effect of the Inclination of a Slope. Four different slope angles, 27°(1:2.0), 34°(1:1.5), 45°(1:1.0) and 63°(1:0.5), are considered in the analysis. The rest of the analysis condition is the same as the one shown in Fig. 8.

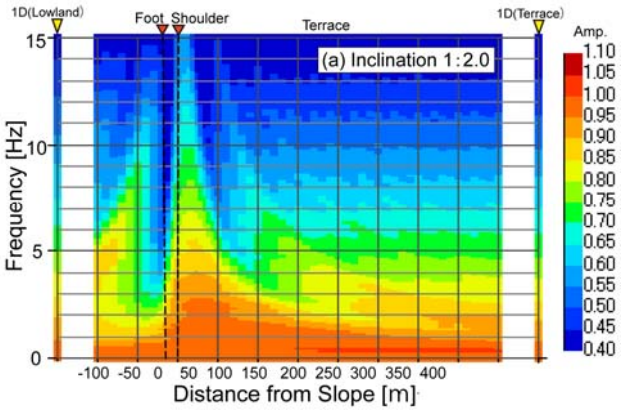

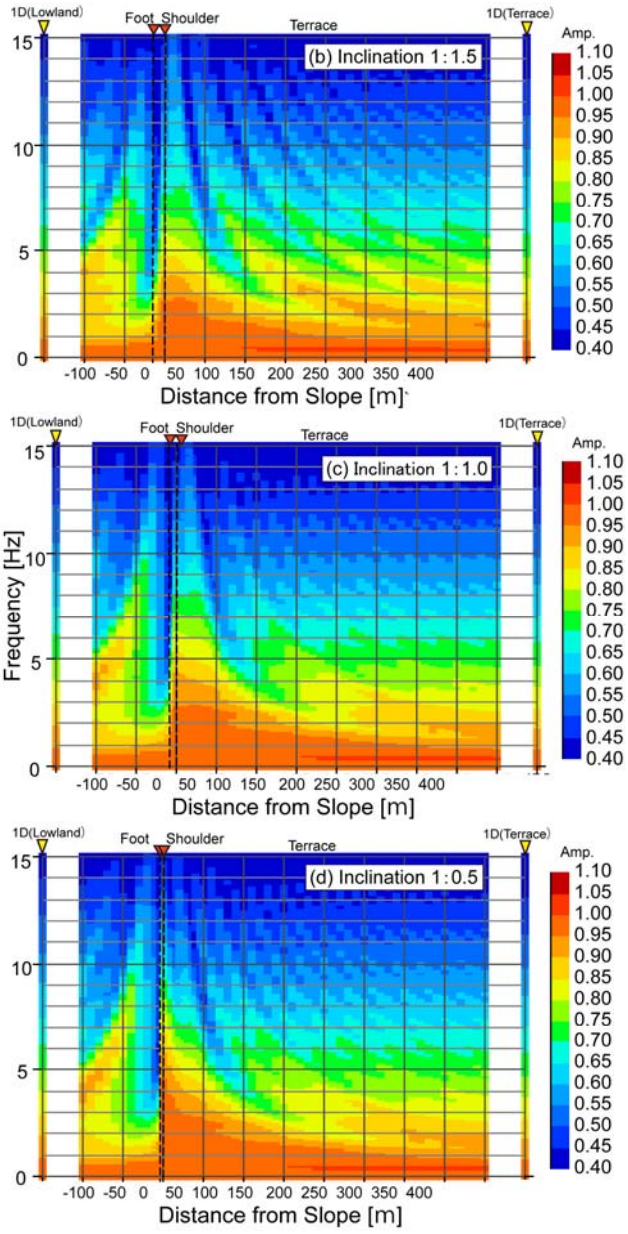

Fig. 11. Distribution of transfer functions on the ground surface (red color indicates larger amplification).

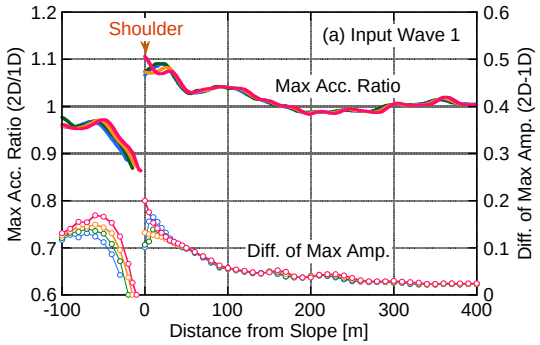

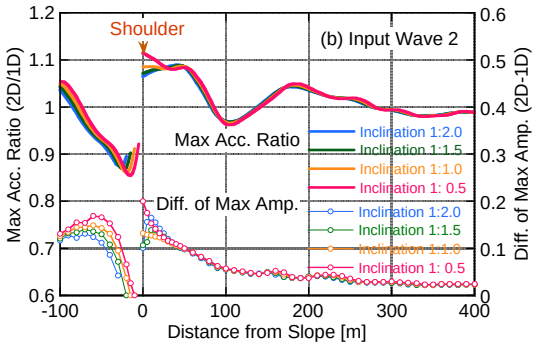

Fig. 12. Distribution of maximum response accelerations on the ground surface (also shown are the differences between 2-D and 1-D analyses).

Figure 11 shows the amplification function on the ground surface with respect to the input motion at the bottom boundary of the model. The effect of inclination of a slope on the dynamic characteristics of the ground is not clear, as shown in this figure. If you take a closer look at this figure, however, it is noted that, larger the inclination, larger the amplitude at the shoulder of the slope. The affected area due to the slope is limited to the terrace and in the vicinity of the shoulder of the slope.

Fig. 12 shows the distribution of the ratio between the maximum acceleration along the ground surface and that of the input wave. In a similar way, the ratio varies depending on the slope inclination, but only in the vicinity of the shoulder of the slope.

Effect of the Stiffness of the Ground. In order to examine the effect of the soil stiffness on the dynamic characteristics, different shear wave velocity cases were considered. Figure 13 shows the distribution of the maximum acceleration ratio along the ground surface. It is shown that the location of the maximum value becomes close to the shoulder when the soil is soft but the difference is not significant.

Summary of the Effect of a Slope. From a series of studies described in this chapter, it can be concluded that the dynamic characteristics of the ground with a slope is influenced by the height of the slope and the stiffness of the ground, but not or little influenced by the angle of a slope. Figure 14 summarizes the principal result of this study as a relationship between the maximum acceleration ratio and the height of the slope.

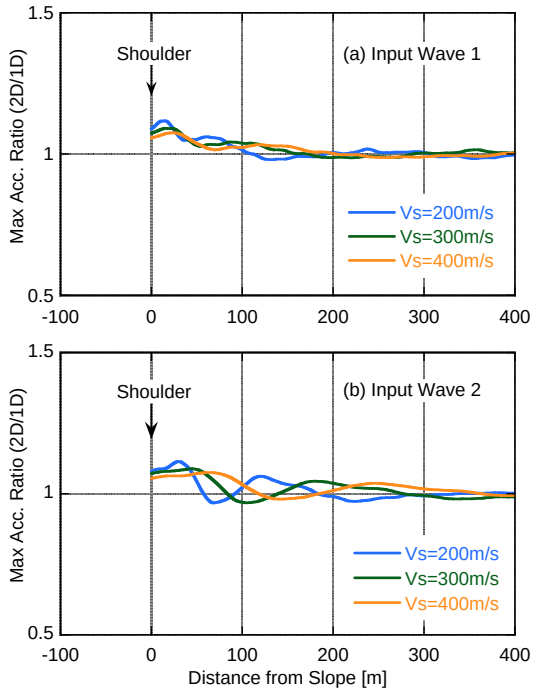

Fig. 13. Distribution of maximum acceleration ratio between 2-D and 1-D analyses (changes due to the soil stiffness).

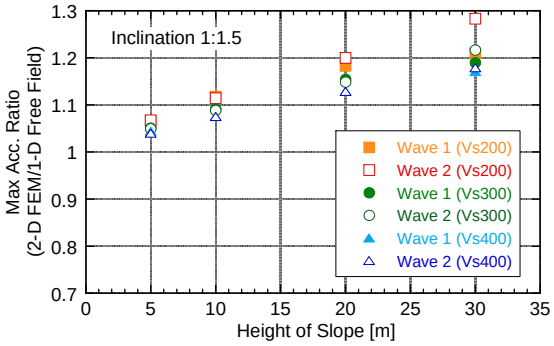

Fig. 14. Relationship between the maximum response acceleration and the height of a slope.

Effect of a Weakened Soil along a Slope

Analysis Model. In order to examine the effect of a weakened soil along a slope on the dynamic characteristics of the ground, a soil model with a weakened part has been analyzed by using finite elements similar to the ones used in the previous section. Figure 15 shows a schematic illustration of the analysis model and Table 3 summarizes the cases considered in the analysis.

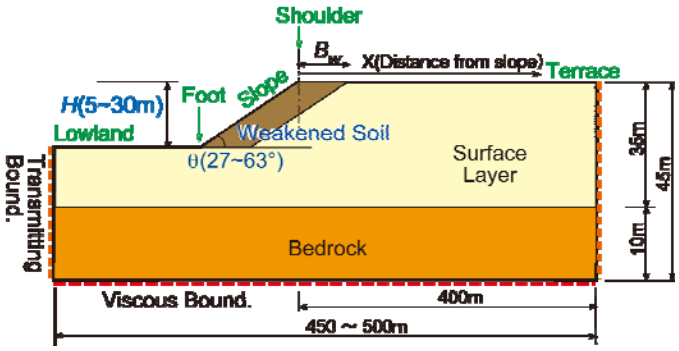

Fig. 15. Schematic illustration of a model used in finite element analyses.

Table 3. Parameters and cases considered in the analyses.

Slope					
		Analysis cases			
Height	H	5m	10m	20m	
Inclination	θ	1:2.0	1:1.5	1:1.0	1:0.5
		26.6°	33.7°	45.0°	63.4°
Soil properties					
		Vs (m/s)	Vp (m/s)	Density (×10³kg/m³)	Damping
Surface layer		150	497	1.8	0.02
		200	663	1.8	0.02
		300	995	1.8	0.02
Bedrock		300	995	1.8	0.02
		400	1327	1.8	0.02

Slope		Transfer function			Max Acc.
H (m)	θ	Vs 150(m/s)	Vs 200(m/s)	Vs 300(m/s)	Vs 200(m/s)
5	1:2.0	o	o	o	-
	1:1.5	o	o	o	o
	1:1.0	o	o	o	-
	1:0.5	o	o	o	-
10	1:2.0	o	o	o	o
	1:1.5	o	o	o	o
	1:1.0	o	o	o	o
	1:0.5	o	o	o	o
20	1:2.0	o	o	o	-
	1:1.5	o	o	o	o
	1:1.0	o	o	o	-
	1:0.5	o	o	o	-

Uniform Ground with a Weakened Soil. Although the ground is usually layered in a real situation, a uniform ground with a weakened part along a slope is considered first.

Figure 16 shows the maximum acceleration distribution on the ground surface. It can be seen that the maximum acceleration is fairly large in the area close to the shoulder of a slope with a weakened soil. However, the area is small, up to about 10 m from the shoulder, beyond this point the effect is not significant.

Figure 17 shows the amplification function at the shoulder of the slope with respect to the input motion at the bottom of the model. In the figure, a one-dimensional analysis result is also plotted, in which the soil model is assumed to be two-layered along the vertical direction at the shoulder of the slope. From this figure, it is pointed out that the two-dimensional analysis gives higher natural frequencies and higher amplifications at the shoulder when compared with the one-dimensional analysis and that its frequency dependency is much more complicated.

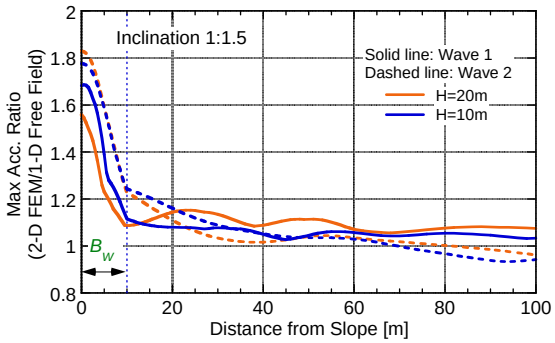

Fig. 16. Distribution of maximum accelerations on the ground surface of a terrace.

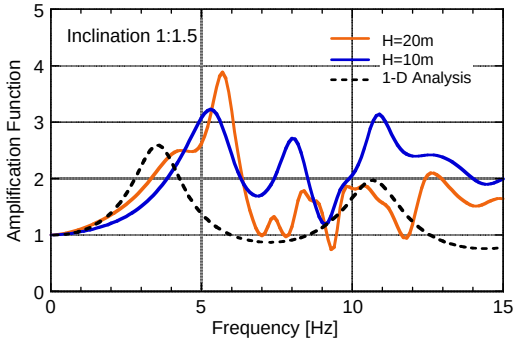

Fig. 17. Comparison of amplification functions among cases with different height of a slope and a 1-D result.

Influence Area of a Weakened Soil. By using a two-layered model, the influence area of the weakened soil has been examined. Figure 18 shows the maximum amplifications on the ground surface with respect to the input wave at the bottom. The shear wave velocity of the surface layer is 200 m/s and that of the underlying halfspace is 400 m/s. It is

shown in this figure that the influence of the weakened soil is large but is limited only to the vicinity of the slope. As mentioned in the previous chapter, the influence of the existence of a slope is small compared to the effect of a weakened soil, but its area of influence is far more broad.

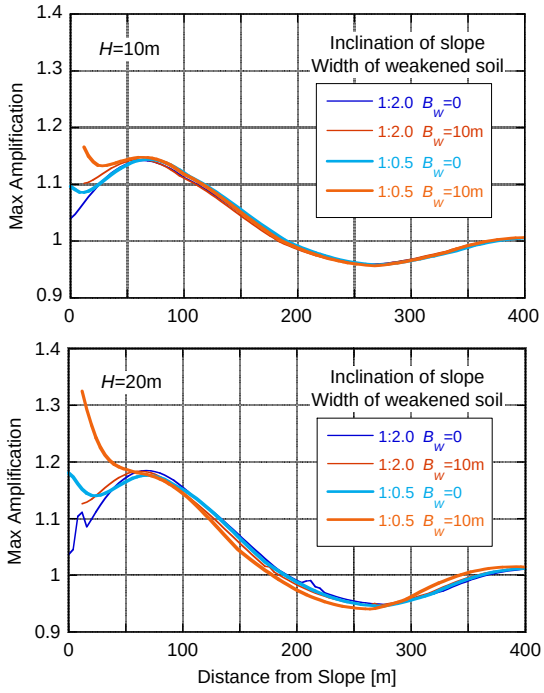

Fig. 18. Variation of maximum values of amplification function with respect to the distance from the shoulder of a slope.

EFFECT OF A WEAKENED SOIL ON THE FAILURE RISK DURING EARTHQUAKES

It has been revealed in the previous chapters that amplification of the ground motion near a slope is observed and its major cause can be attributed to the existence of a weakened soil along the slope. In this chapter, a seismic risk from the viewpoint of slope failure during earthquakes is examined by conducting elasto-plastic finite element analyses in time domain.

Analysis Method and Model

Analysis Method. Two-dimensional elasto-plastic finite element analyses have been carried out. The analysis model has dashpots at the boundaries and the Rayleigh damping was assumed as material damping. As a constitutive relation, the so-called modified Ramberg-Osgood model was used, in which the shear stress and strain relationship is expressed by the following expressions (Yoshimi and Fukutake, 2005):

$$\gamma = \frac{\tau}{G_0}\left(1+\alpha|\tau|^{\beta}\right) \tag{1}$$

$$\alpha = \left(\frac{2}{\gamma_{0.5}G_0}\right)^{\beta} \qquad \beta = \frac{2\pi h_{\max}}{2-\pi h_{\max}} \tag{2}$$

where, γ is the shear strain, τ is the shear stress, G_0 is the initial shear stiffness, h_{max} is the maximum damping factor, $\gamma_{0.5}$ is the reference shear strain and α, β are the model parameters.

The analysis starts with the application of gravity loads, in which the initial properties of the soil is determined by the following expressions:

$$G_0 = G_{0i}\left(\frac{\sigma'_m}{\sigma'_{mi}}\right)^{n_1} \tag{3}$$

$$\gamma_{0.5} = \gamma_{0.5i}\left(\frac{\sigma'_m}{\sigma'_{mi}}\right)^{n_2} \tag{4}$$

where, parameters n_1 and n_2 are set to 0.5 and G_{0i} and $\gamma_{0.5i}$ are computed from the mean stress of σ'_{mi}.

Analysis Model. The analysis model is similar to the one used in the previous analysis except that the viscous boundary was assumed at the both sides of the model in addition to the bottom boundary. Table 4 summarizes the parameters used in the analysis. The input motion was defined as an upward incident wave at the bottom of the model. Two ground motions were considered as in the case of elastic analysis described in the previous chapter.

Table 4. Soil parameters.

Soil Properties		Weakened Soil				Surface Soil	Bedrock
Condition	Height [m]	10	10	10	20	-	-
	Inclination	1:2.0	1:1.5	1:1.0	1:2.0		
Initial Shear Stiffness G_{0i}		86,980	88,470	75,720	81,650	13,455	288,000
Density [x10^{3}kg/m^3]		1.8					
Poisson's Ratio n		0.45					
Maximum Damping h_{max}		0.24					-
Reference Strain $g_{0.5i}$		0.001158					-
n_1		0.5					0
n_2		0.5					0
Rayleigh Damping	α	0.000749					
	β	0.22176					

Result of Gravity Load Analysis. Figure 19 shows the distribution of initial shear wave velocity in the model based on the gravity load analysis. It is noted that, since the stiffness depends on the initial stress due to gravity, the equivalent shear wave velocity is small near the ground surface and large in the deeper ground. Thus the existence of a weakened soil is a little hard to recognize. In fact, the difference of the shear

wave velocity between adjacent two finite elements along the boundary is about 50 m/s.

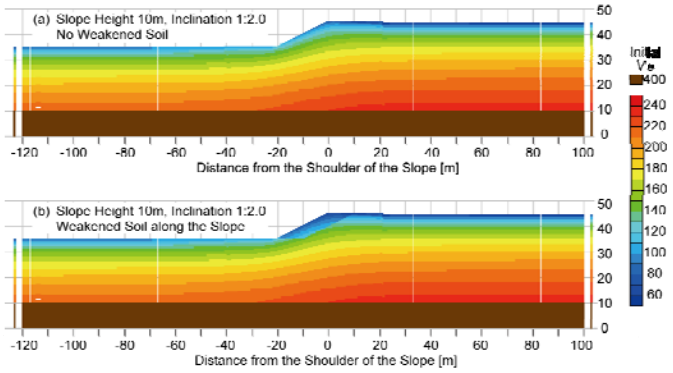

Fig. 19. Distribution of initial shear wave velocity based on the gravity load analysis.

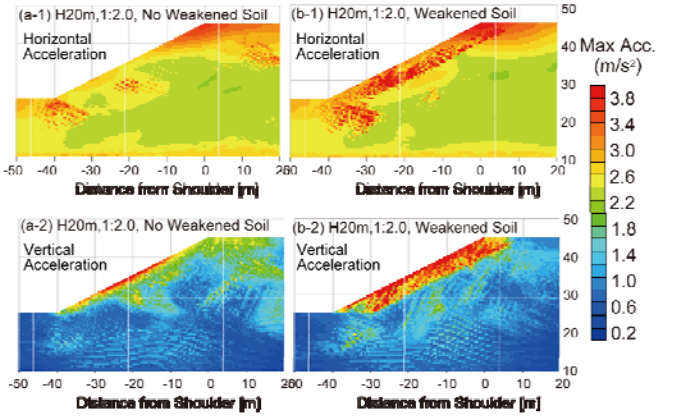

Fig. 20. Comparison of maximum response accelerations between the case without weakened soils and the one with weakened soils along the slope.

Effect of a Weakened Soil on the Slope Failure Risk

Maximum Accelerations. Figure 20 shows some of the analysis results. From this figure and other results not shown in this paper due to space limitations, it can be pointed out the followings:

- Due to a weakened soil, accelerations along a slope, especially in the vertical direction, become large.
- The shape of the slope (height and angle) does not have a significant influence on accelerations along the slope, except in the case of a large height in which accelerations become large inside the weakened soil.
- The distribution of maximum accelerations in the ground is dependent on the type of input waves, most probably its frequency content.

Maximum Velocities. Unlike accelerations, the effect of the weakened soil on the distribution of the maximum velocity is fairly small. The possible reason for this is that, although the ground motion is amplified inside the weakened soil, its frequency component is large only in the higher frequency range and not in the lower range.

Maximum Shear Strains. Maximum shear strains during an earthquake has been computed by the following expression:

$$\gamma_{\max} = \sqrt{\left(\varepsilon_x - \varepsilon_y\right)^2 + \gamma_{xy}^{\ 2}} \tag{5}$$

where, ε is the normal strain and γ is the shear strain.

Since the soil properties in this analysis are dependent on the confined pressure in the ground, the difference between the initial condition of the weakened soil model and that of the model without the weakened soil is relatively small, as mentioned earlier. However, analysis results are quite different from the viewpoint of the shear strain distribution in the ground.

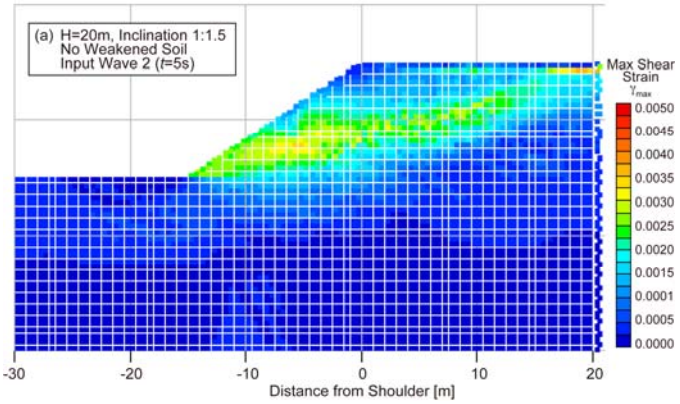

Fig. 21. Example of shear strain distribution near the slope without weakened soils (input wave 2, at time 5 s).

Figure 21 shows the shear strain distribution for the case of no weakened soil model, while Fig. 22 shows that of the weakened soil model case. The comparison between these two figures in addition to other comparisons among a variety of analysis results, it is possible to point out the followings:

- Without weakened soils along a slope, no significant concentration of large shear strains is observed in the ground.
- However, depending on the type of input waves, there is a case in that a circular pattern of fairly large shear strains appears near the slope, indicating the possibility of a circular failure of the ground at the slope.
- In the case of a slope with a weakened soil, very large strains are developed throughout the weakened soil,

meaning that there is a high possibility of slope failure occurring in this part of the slope.
- These tendencies depend on the type of input ground motions, due probably to the difference of frequency contents.

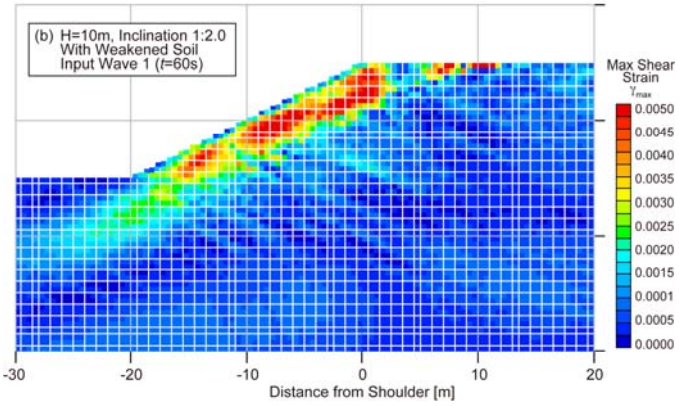

Fig. 22. Example of shear strain distribution near the slope with weakened soils (input wave 1, at time 60 s).

CONCLUSIONS

In this study, the dynamic characteristics of the ground near a slope located at the edge of a diluvial terrace have been examined in detail. Based on the results, the followings can be pointed out.

- The ground motion during an earthquake is smaller at the foot of a slope but larger at its shoulder.
- The effect of a slope itself on the dynamic characteristics is relatively small from the viewpoint of amplification but its influence area is fairly large.
- The existence of a weakened soil along the slope plays a very important role in the dynamic characteristics of the ground in that the ground motion is amplified by a great deal and the maximum strain becomes very large near the slope.
- However, its influence area is limited to the vicinity of the slope.

REFERENCES

Asano, S., Matsuura, S., Okamoto, T. and Matsuyama, K. [2003]. "Shaking table tests to measure the underground displacement of the slope", Journal of the Japan Landslide Society, Vol. 40, No. 2, pp. 30-33. (in Japanese)

Building Research Institute and Japan Institute of Construction Engineering. [1995]. "Development of Technology for Earthquake Disaster Prevention", Report. (in Japanese)

Asano, S., Ochiai, H., Kurokawa, U. and Okada, Y. [2006]. "Topographic effects on earthquake motion that trigger landslides", Journal of the Japan Landslide Society, Vol. 42, No. 6, pp. 1-10. (in Japanese)

Chiba Prefectural Government. [1980]. "*Fundamental research on landform classification Chiba*" (in Japanese).

Hayakawa, T. [1996]. "Characteristics of Seismic Response of Slopes and Topographic Effects
Evaluation", Proc. AIJ Annual Convention, Vol. B, pp. 263-264. (in Japanese)

Kobayashi, T., Nakamura, S. and Yoshida, R. [1993]. "Study on Evaluation of Design Earthquake Ground Motion for Buildings (Part 6: Evaluation of Ground Motion's Property Affected by Irregularity of Local Site Topography and Geology)", Proc. AIJ Annual Convention, Vol. B, pp. 127-128. (in Japanese)

Kurita, T., Annaka, T., Takahashi, S., Shimada, M. and Suehiro, T. [2005]. "Effect of irregular topography on strong ground motion amplification", Journal of Japan Association for Earthquake Engineering, Vol. 5, No. 3, pp. 1-11. (in Japanese)

Matsuoka, M. and Midorikawa, S. [1994]. "The Digital National Land Information and seismic microzoning", Proc. 22nd Symposium on Ground Vibration, Architectural Institute of Japan, pp. 23-34. (in Japanese)

Nagata, Y., Nakai, S., Funahashi, Y. and Ishida, R. [2006]. "Dynamic properties of the edge of diluvial terrace", *Proc. 12th Japan Earthquake Engineering Symposium*, pp. 702-705. (in Japanese)

Nagata, Y., Nakai, S. and Sekiguchi, T. [2008]. "Study of the slope effect on the dynamic properties of dilluvial terrace", Journal of Japan Association for Earthquake Engineering, Vol. 8, No. 4, pp. 1-11. (in Japanese)

Nakai, S., Yamaguchi, S. and Ishida, R. [2002]. "Estimation of soil conditions based on land use in the old times and satellite data", Journal of Structural and Construction Engineering, Transactions of AIJ, No. 552, pp. 69-75. (in Japanese)

Nakai, S., Ishida, R., Dejun, Y. and Nagata, Y. [2004]. "A study on the site characterization of complex micro landform", *Proc. 13th World Conference on Earthquake Engineering*, Paper No. 2257.

Wang, W., Nakamura, H., Tuchiya, S., Wu, S. and Ouyang, S. [2004]. "Occurrences and displacements of landslides by an earthquake with a subsequent rain: the 1999 Chi-chi earthquake in central Taiwan", Journal of the Japan Landslide Society, Vol. 41, No. 4, pp. 44-52.

Yoshimi, Y. and Fukutake, K. [2005]. "Physics, Evaluation and Countermeasures of Liquefaction", Gihodo Shuppan. (in Japanese)